SMGroup

SM Journal of Gastroenterology & Hepatology

Research Article

# Rodent Hepatocellular Carcinoma Cells Found in Hepatic Veins Do Not Necessarily Colonize the Lung: Observations in Line with the "Seed and Soil" Hypothesis

**Yewei Liu[1,2], Ting Yin[1], Yuanbo Feng[1], Feng Chen[1], Jie Yu[1], Jianjun Liu[2], Shaoli Song[2], Uwe Himmelreich[1], Raymond Oyen[1], Gang Huang[2,3,4]* and Yicheng Ni[1]***

*[1]Department of Imaging and Pathology, Faculty of Medicine, KU Leuven, Leuven 3000, Belgium*
*[2]Institute of Clinical Nuclear Medicine, Renji Hospital, Shanghai Jiao Tong University School of Medicine, Shanghai 200127, China*
*[3]Institute of Health Sciences, Shanghai Jiao Tong University School of Medicine (SJTUSM) & Shanghai Institutes for Biological Sciences (SIBS), Chinese Academy of Sciences (CAS), Shanghai 200025, China*
*[4]Shanghai University of Medicine and Health Sciences, Shanghai 201318, China*

**Article Information**

Received date: Oct 03, 2016
Accepted date: Dec 21, 2016
Published date: Dec 26, 2016

***Corresponding author(s)**

Yicheng Ni, Department of Imaging and Pathology, Faculty of Medicine, KU Leuven, Herestraat 49, Leuven 3000, Belgium, Tel: +32-16-330165; Fax: +32-16-343765; Email: yicheng.ni@med.kuleuven.be

Gang Huang, Department of Nuclear Medicine, Renji Hospital, Shanghai Jiao Tong University, School of Medicine, Shanghai 200127, China, Tel: +86-21-33755258; Fax: +86-21-65882195; Email: huang2802@163.com



**Keywords** Primary live cancer; Hepatocellular carcinoma; Hepatic vein thrombosis; Vasculogenic mimicry; Magnetic resonance imaging

## Abstract

Hepatocellular Carcinoma (HCC) is the most common subtype of primary liver cancer. Diethylnitrosamine (DENA) can induce multifocal primary liver tumors in rodents, which is a valuable animal model because of its close resemblances to human primary liver cancers in terms of disease progression and histopathological features such as the variety of cellular subtypes and differentiation. In this article, we present a rat example with DENA-induced primary liver cancer, which developed a shortness of breath. Magnetic Resonance Imaging (MRI) using two different Contrast Agents (CAs) Gadoterate meglumine (Gd-DOTA) and Mangafodipir trisodium (Mn-DPDP) revealed three liver masses and multiple pulmonary nodules. A diagnosis of HCC with suspected lung metastases was suggested, which seemed to be supported by the autopsy that proved the presence of both hepatic and pulmonary lesions as shown by MRI. Microscopically, hematoxylin and eosin (H&E) stained slices identified three primary angioma-like HCCs with tumor invasion and emboli in the lumens of intrahepatic veins, but the lung masses turned out to be inflammatory nodules secondary to chronic bronchitis. In addition, Immunohistochemical (IHC) staining of HCC markers hepatocyte paraffin antigen-1 (HepPar1) and glypican-3 (GPC3) showed slight positivity in the floating tumor cells both in the parent tumors and in the intrahepatic vein branches. Therefore, lung metastases of HCC were excluded in this case, which is in line with the old "seed and soil" hypothesis for malignant metastases. Finally, this phenomenon, the related causes and clinical significance are discussed.

## Introduction

HCC shows a high predilection for vascular invasion [1]. As a common complication, Portal/Hepatic Vein Tumor Thrombosis (PVTT/HVTT) of HCC is considered as a sign of advanced stage and an adverse prognostic factor [1,2]. In patients, PVTT is present in 10-40% of HCC at the moment of diagnosis, which may occur as the initial sign of an undetected HCC or as an indicator of recurrence after treatment [2]. The main sites of extrahepatic spread are lungs, abdominal lymph nodes and bones [3]. Lung (39-55%) is the most common target of extrahepatic HCC metastasis via hematogenous dissemination [3-5], because HCC cells downstream in the blood circulation tend to easily settle down in the lung through the pulmonary artery system [5]. Generally, both intrahepatic and extrahepatic metastases tend to occur in poorly differentiated HCC with an aggressively diffuse growth pattern.

Diethylnitrosamine (DENA)-induced hepatocarcinogenesis in rats is a valuable animal model because of its high analogy to the histopathological progression observed in human liver cancer, including general liver cirrhosis, dysplastic nodules and multifocal malignant liver tumors [6]. Furthermore, a full spectrum of HCCs in varied differentiation and vascularity can be observed as the main subtype [7].

In this paper, we present a case of DENA-induced primary HCC in Sprague Dawley (SD) rats with evidenced hepatic vein invasion and suspected pulmonary metastases by *in vivo* Magnetic Resonance Imaging (MRI), but the pulmonary metastatic disease could be excluded by careful histopathological exams. Moreover, contrary to the common belief, the degree of cellular differentiation of the HCC found in HVTT was not extremely poor. These experimental observations are discussed cross-referencing the literature.

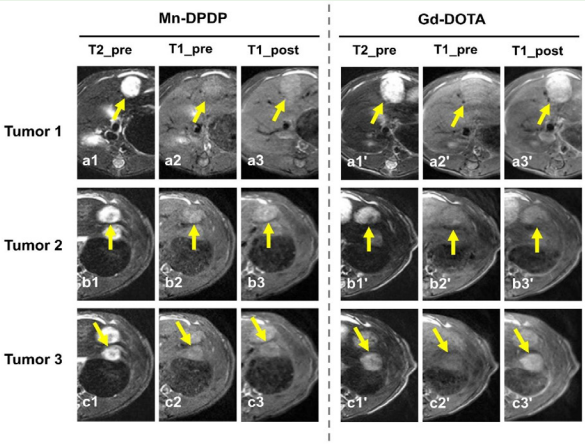


**Figure 1:** MR image diagnosis of 3 HCCs. T2WI showed three liver tumors (arrows) with hyper-intensity located in the median lobe right part (a1, a1'), the median lobe left part (b1, b1') and the left lobe (c1, c1'). T1WI showed 3 lesions (arrows) with slightly hyper-intensity (a2-c2, a2'-c2'). Twenty-four hours after Mn-DPDP administration, the lesions (arrows) were mildly enhanced (a3-c3). Immediately after Gd-DOTA injection, contrast enhanced images showed the lesions (arrows) with high enhancement (a3'-c3').

## Animal Experiments

Over 60 male SD rats at the age of 8 weeks were administrated daily with DENA gavage feeding at a dose of 10 mg/kg body weight for 8 weeks. MRI was used weekly to monitor liver tumor growth from the 9th week until the largest liver tumor reached 1cm in diameter, ready for further preclinical theragnostic research. Among them, one rat got shortness of breath especially during MRI scanning when it was under gas anesthesia [8]. Contrast Enhanced MRI (CE-MRI) was then performed to further characterize these liver lesions by using a non-specific MRI Contrast Agent (CA) Gadoterate meglumine (Gd-DOTA), and a hepatobiliary CA Mangafodipir trisodium (Mn-DPDP). For postmortem digital microangiography, hepatic artery was perfused with barium sulfate before liver specimen was radiographed. Then liver specimen was resected, fixed in formalin, bedded in paraffin, sliced into 5 $\mu$m and stained with H&E as well as immunohistochemical markers for HCC including hepatocyte

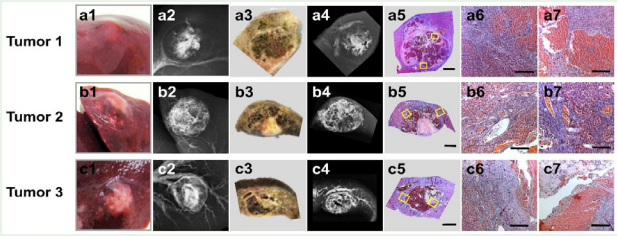


**Figure 2:** Pathological specimen, microangiographic and microscopic results of 3 HCCs. The photomacrographs of the liver samples (a1-c1) and the sectioned lesions (a4-c4) demonstrated 3 roughly spherical tumors. From digital micrography of the entire tumors (a2-c2) and the sectioned lesions (a4-c4), tumor vessels and enlarged intratumoral vascular lakes were perfused by barium sulfate. Microscopically, the HCCs were highly vascularized, capsuled or circumscribed by fibrosis, and contained spontaneous necrosis on the general background of liver cirrhosis (a5-c5, H&E staining, × 12.5 original magnification, scale bar = 800 $\mu$m; a6-a7, b6-b7, c6-c7, H&E staining, × 100 original magnification, scale bar = 100 $\mu$m).

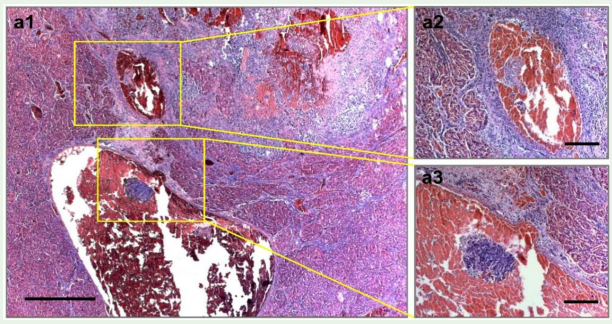


**Figure 3:** Evidence of vascular invasion in tumor 1. H&E stained microphotographs demonstrated the tumor thrombosis invading hepatic veins (a1, × 25 original magnification, scale bar = 400 $\mu$m; a2-a3, × 100 original magnification, scale bar = 100 $\mu$m).

paraffin antigen-1 (HepPar1) and Glypican-3 (GPC3). Meanwhile, other organs including the lung were collected and fixed as well.

Liver T2-Weighted (T2WI) MRI demonstrated three tumor lesions located in the right and left part of the median lobe, and in the left lobe, measuring 1.01×0.86 cm, 0.92× 0.72 cm, 0.74×0.68cm in size, respectively (Figures 1a1'-c1'). All three tumors appeared hyperintense on T2WI (Figures 1a1-c1, a1'-c1'), slightly hyperintense on T1WI (Figures 1a2-c2, a2'-c2'), and were strongly enhanced on GD-DOTACE-MRI (Figures 1a3'-c3'), suggesting their hypervascular nature. Twenty-four hours after Mn-DPDP injection, all three tumors generally appeared mild hyperintense (Figures 1a3-c3). This not only suggested that they were differentiated HCCs [9], but also indicated that they were not dense with cancer cellularity but rich in vascularity. Additionally, in tumor 2, there was a triangular region appearing hypointense on T2WI (Figure 1b1'), slightly hyperintense on T1WI (Figure 1b2'), unenhanced by Gd-DOTA (Figure 1b3'), and surrounded by a highly enhancing rim with Mn-DPDP (Figure 1b3). Whereas, tumor 3 showed a central hypointense core on T2WI (Figure 1c1'), which became unenhanced by both Gd-DOTA (Figure 1c3') and Mn-DPDP (Figure 1c3).

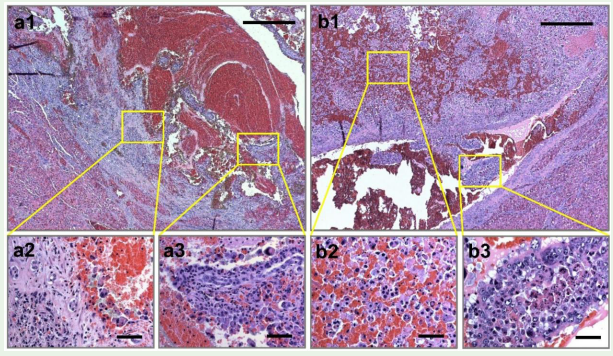


**Figure 4:** Two different clusters of malignant cells appeared in one HCC lesion. H&E stained microphotographs revealed both the moderate-to-high differentiated HCC cells (a1, a3, b1, b2) floating in the vascular lakes and the fibroblast-like tumor cells (a1, a2) forming the bank of vascular lakes. Noticeably, the HCC cells in the tumor thrombosis in the hepatic vein (b3) appeared higher N/C ratio and brisker mitotic activity (a1-b1, H&E staining, × 50 original magnification, scale bar = 200 $\mu$m; a2-a3, b2-b3, H&E staining, × 400 original magnification, scale bar = 25 $\mu$m).

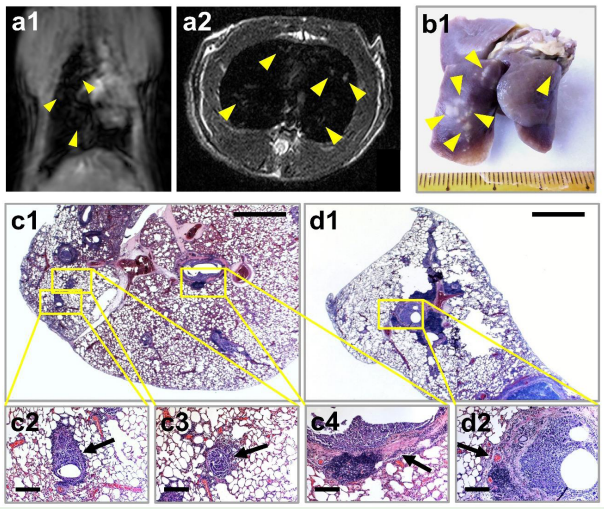


**Figure 5:** Multiple scattered pulmonary masses revealed by MRI and verified by autopsy and H&E staining. Coronal (a1) and transverse (a2) T2WI identified numerous pulmonary nodules distributed in different lung lobs. The photomacrograph showed multiple whitish nodules scattered in the lung lobes (b1). Microphotograph of the H&E-stained paraffin section of multifocal pulmonary masses (c1, d1, × 12.5 original magnification, scale bar = 800 μm; c2-c4, d2, × 100 original magnification, scale bar = 100 μm). These nodules (arrows) showed the mononuclear cell infiltration inside a layer of simple ciliated columnar epithelium (c2, c3), surrounded by a rim of fibrosis, and even with lyphocytic infiltration (c4, d2).

From macroscopic appearance of liver, three liver tumors were identified (Figures 2a1-c1). The cut surfaces of these masses revealed three well defined, highly vascularized and circumscribed tumors (Figures 2a3-c3), two of which contained eccentric yellowish-white-colored spontaneous necrosis (Figures 2b3-c3) corresponding to the heterogeneous components observed by MRI in tumor 2 and 3. From digital microangiography, all the 3 lesions showed hypervascularity, as the tumor vessels and vascular lakes were filled with barium suspension (Figures 2a2-c2). Sliced sections (Figures 2a4-c4) appeared hyperdense as well on the radiography, which was in accord with the findings on GD-DOTA CE-MRI. Microscopically, all of the three masses revealed enlarged lake-like blood spaces separated by hypocellular fibrous septa (Figures 2a5-a7,b5,c5), thickly capsuled (Figures 2a5-a6, c5-c6) or circumscribed (Figures 2b5-b7) by fibrous on general liver cirrhosis background (Figures 2a5-c5); and both tumor 2 and 3 contained spontaneous necrosis/thrombosis (Figures 2b5, c5, c7). Moreover, the banks of vascular lakes were lined up directly by HCC cells rather than endothelial cells (Figures 2a6-a7, 2c6-c7). This phenomenon is named Vasculogenic Mimicry (VM) [10]. The presence of red blood cells and perfused barium sulfate indicated that blood circulates in these VM vessels (Figures 2a5-a7, b5-b7, c5-c7). On top of that, from H&E staining, tumor thrombi were frequently identified invading the hepatic veins in tumor 1 (Figure 3).

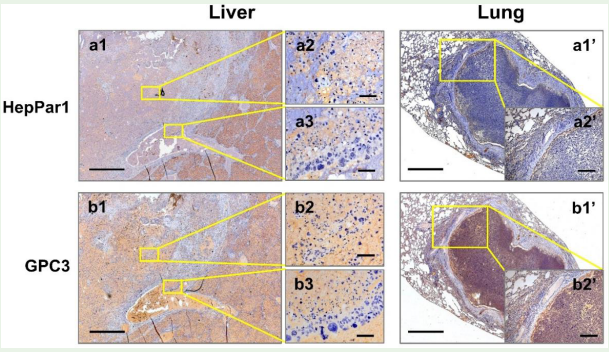


**Figure 6:** Expression of HCC markers HepPar1 and GPC3 in rat liver tumors and lung samples. Malignant liver tumor lesions were identified by slightly positive staining in the floating tumor cells and negative staining in the surrounded fibroblast-like tumor cells for HepPar1 (a1-a3, upper left panel) and GPC3 (b1-b3, lower left panel); lung lesions showed relatively negative staining for HepPar1 (a1'-a2', upper right panel) and non-specific positive staining for GPC3 (b1'-b2', lower right panel). (a1, a1', b1, b1', IHC staining, × 25 original magnification, scale bar = 400 μm; a2-a3, b2-b3, IHC staining, × 400 original magnification, scale bar = 25 μm; a2'-b2', IHC staining, × 100 original magnification, scale bar = 100 μm).

As further revealed by high-magnification images, there were two main different clusters of cancer cells in the parent HCC lesions. Firstly, the floating tumor cells of moderate-to-high differentiation appeared to be responsible for tumor cell extravasation via a series of sequential steps including detaching from the extracellular matrix and gaining access to the blood circulation due to the venous drainage (Figure 4a1, a3, b1, b2), which could be attributed to the suspected pulmonary metastases as detected by MRI (Figures 5a1-a2). Secondly, the fibroblast-like tumor cells not only contributed to forming the bank of vascular lakes allowing the HCC cells to attach with, but also invaded the surrounding cirrhotic liver tissue in a reticular growth pattern in the meantime (Figures 4a1-a2). All these mixed subpopulations of aggressive HCC cells displayed the malignant characteristics such as pleomorphism, cytological atypia, brisk mitotic activity, high Nucleus-to-Cytoplasm (N/C) ratio and occasionally discovered multinucleated giant cells (Figures 4b1-b3).

In the lung, multiple visible nodules in varied sizes were scattered in the left and right lobes, as revealed by T2WI (Figures 5a1-a2). This was corresponded to the dozens of solid pulmonary lesions found at autopsy (Figure 5b1), which supported the initial impression of multiple lung metastases of HCC. However, none of those pulmonary nodules were microscopically of malignant features and hepatic origins. Instead, dense mononuclear cells frequently infiltrated in the bronchi and/or bronchioles together with the proliferated pulmonary epithelia (Figures 5c1, d1), which were surrounded by fiber texture and lymphocytic infiltration (Figures 5c2-c4, d2), leading to a final diagnosis of chronic bronchitis for the pulmonary lesions.

Immunohistochemical analysis of clinical diagnostic makers of HCC indicated that the floating tumor cells both in the parent tumors and as the tumor thrombi were slightly positive for hepatocyte paraffin antigen-1 (HepPar1) and glypican-3 (GPC3) (Figures 6a1-a3, b1-b3). Meanwhile, a subpopulation of aggressive HCC cells in the tumor thrombi were nearly negatively stained indicative of their lower cellular differentiation (Figures 6a3, b3). However, the pulmonary masses were non-specifically positively stained for GPC3 as well (Figures 6b1'-b2'), whereas HepPar1 staining was relatively negative (Figures 6a1'-a2').

Considering the histopathological characteristics, immunohistochemical features of the lesions and the success of this rat model, a diagnosis of multiple HCCs with hepatic vein invasion excluding pulmonary metastases was established for this rat.

## Discussion

Upon a clinically translational setting that facilitates co-localization of MRI and histology findings [11], in this rat case, DENA-induced primary HCCs with hepatic vein invasion was the final most reasonable diagnosis which is based on the common cytopathological features and HCC marker expression shared by the parent HCC lesions as well as the floating moderate-to-high differentiated HCC cells inside tumoral vascular lakes and the tumor thrombi invading the hepatic veins. Regardless of non-specific positive staining with the HCC markers, the pulmonary nodules were eventually excluded from the diagnosis of lung metastasis of HCC as evidenced by the inflammatory cellular morphology by H&E staining, and were further defined as the symptomatic chronic bronchitis with nodular respiratory inflammation and epithelial proliferation.

Theoretically, the tumor emboli in the hepatic veins shed from a liver cancer may spread hematogenously into the lung rather easily via the inferior vena cava, right atrium and ventricle of the heart, and pulmonary arteries, and consequently cause extensive pulmonary metastases. However, the lung metastases are only identified in 39-55% patients, although the lung is the most frequently site of extrahepatic metastasis [5]. This suggests that, in spite of the physical dissemination of tumor cells from the parent tumor to distant tissues, whether metastasis forms still depends on the adaptation of the metastasizing tumor cells to the discrete microenvironments [12]. This is in line with the "Seed and Soil" hypothesis proposed by Stephen Paget back to 1889, denoting that certain tumor cells, the "seeds", grow preferentially in the stroma of selected organs, the "soil" [13]. In one study, only less than 0.01% of Circulating Tumor Cells (CTCs) eventually manage to survive and form a secondary cancer [14]. Much higher lung metastatic rate (50-80%) was found in another study using an implantable HCC tumor cell line [15], suggesting the aggressivity of CTCs also matters in metastatic colonization. There are a large number of complex and diverse cell-biological mechanisms underlying CTC's capability of adapting remote tissue microenvironments to form macroscopic tumors, such as the ability to activate angiogenesis, tumor-suppressing actions by the immune system or anti-growth signals embedded in normal tissue extracellular matrix, etc [12]. These findings can also help to explain our findings that the observed pulmonary nodules were eventually excluded as HCC metastasis from primary liver cancer, despite the numerous metastatic tumor thrombi found the hepatic vein branches.

At the aspect of tumor "seeds", progressively acquired genomic instability is an essential driving force for metastasis [16], which is recently considered to be carried out by the existence of a minor subpopulation of cells, namely Cancer Stem Cells (CSCs), through their capacity to self-renew, produce heterogeneous progeny and limitlessly divide [17-19].This phenomenon was also illustrated in our case by the more malignant cluster of tumor cells consisting of the tumor thrombosis in hepatic vein. Practically, by the expression of CSC markers such as CD44, CD133, CD90, ALDH and EpCAM, liver CSCs can be further identified [18,19]. In addition, in order to regulate and maintain the stemness of liver CSC, multiple signals have been altered, like EpCAM, Wnt/$\beta$-catenin pathway, the Sonic Hedgehog pathway, and the Notch pathway [18]. Consistently, DENA-induced mouse HCCs were discovered to be closely clustered with those from MycTgfa transgenic mice by gene expression profile; furthermore, their gene expression patterns were most similar to those of the poorer survival group of human HCCs [20].

Notably, biological heterogeneity has been widely observed in many human and animal tumors at the time of diagnosis, since numerous subpopulations of cells, bearing various biological characteristics like metastatic potential, can been identified in one lesion [21]. In the parent HCC lesions of our case, there were two main different clusters of cancer cells, the floating tumor cells, which appeared to be responsible for tumor cell extravasation via a series of sequential steps including detaching from the extracellular matrix and gaining access to the blood circulation due to the venous drainage, and the fibroblast-like tumor cells, which not only contributed to form the bank of vascular lakes allowing the HCC cells to attach with, but also invaded the surrounding cirrhotic liver tissue in a reticular growth pattern in the meantime.

Vasculogenic Mimicry (VM) refers to the phenomenon that aggressive tumor cells simulate endothelial cells to directly line up vasculogenic structure, which has been increasingly discovered in various solid tumor types [22,23]. Accumulated evidence have shown that VM in HCC tends to be associated with higher tumor grade, metastasis and even poorer overall survival [23,24]. As shown in this study, DENA-induced HCC in rats could be an ideal animal liver cancer model for studying VM [25].

Puzzles do remain in this study and need to be answered by further research. For instance, abundant CTCs appeared floating in the tumoral vascular lakes or in the lumens of hepatic vein branches, but they disappeared from the lung. What was the fate of those CTCs released by the HCCs? Where did they go? Were they still alive somewhere in the body? Or had they already died by the mediated cytolysis or phagocytosis in the blood stream? Answering these questions may enable better understanding of the molecular, cellular and pathophysiological mechanisms of tumorigenesis; invasion and metastases.

In summary, we described a case in rats with DENA-induced hypervascular HCCs with the evident hepatic vein invasion. By H&E staining and IHC staining with HCC markers HepPar1 and GPC3, the primary HCC was diagnosed, but the secondary pulmonary metastasis could be excluded, suggesting that abundant HCC cells found in hepatic vein branches do not inevitably lead to lung metastasis. Moreover, DENA-induced primary liver cancer model can not only simulate the several stages as seen with the clinical HCC patients, but also provide a very rare histologic HCC subtype, angioma-like HCC, which is particularly valuable in the future research regarding VM and hematogenous tumor migration and progression.

## Acknowledgments

This work has partially been supported by KU Leuven projects IOF-HB/08/009 and IOF-HB/12/018, the KU Leuven Molecular Small Animal Imaging Center Mosaic (KUL EF/05/08) and European Union (Asia-Link CfP 2006-EuropeAid/123738/ACT/Multi-Proposal No. 128-498/111); and by research grants from "973" Project (2012CB932604), New Drug Discovery Project (2012ZX09506-001-005), the National Natural Science Foundation of China (Grant No. 81530053, 81471685). Liu YW is sponsored by a scholarship from the center of excellence *In vivo* Molecular Imaging Research (IMIR). The corresponding author is a Bayer Lecture Chair holder.

## References

1. Shaohua L, Qiaoxuan W, Peng S, Qing L, Zhongyuan Y, Ming S, et al. Surgical Strategy for Hepatocellular Carcinoma Patients with Portal/Hepatic Vein Tumor Thrombosis. PLoS One. 2015; 10: e0130021.
2. Quirk M, Kim YH, Saab S, Lee EW. Management of hepatocellular carcinoma with portal vein thrombosis. World J Gastroenterol. 2015; 21: 3462-3471.
3. Natsuizaka M, Omura T, Akaike T, Kuwata Y, Yamazaki K, Sato T, et al. Clinical features of hepatocellular carcinoma with extrahepatic metastases. J Gastroenterol Hepatol. 2005; 20: 1781-1787.
4. Katyal S, Oliver JH, Peterson MS, Ferris JV, Carr BS, Baron RL. Extrahepatic Metastases of Hepatocellular Carcinoma. Radiology. 2000; 216: 698-703.
5. Zhang SM, Zeng ZC, Tang ZY, Sun J, Cheng JM, Liu R, et al. Prognostic analysis of pulmonary metastases from hepatocellular carcinoma. Hepatol Int. 2008; 2: 237-243.
6. Yang FC, Zheng SS, Jiang TA. A modified rat model for hepatocellular carcinoma. Hepatobiliary Pancreat Dis Int. 2004; 3: 585-587.
7. Ni Y, Marchal G, Yu J, Mühler A, Lukito G, Baert AL. Prolonged positive contrast enhancement with Gd-EOB-DTPA in experimental liver tumors: Potential value in tissue characterization. J Magn Reson Imaging. 1994; 4: 355-363.
8. Liu YW, Yin T, Feng YB, Chen F, Yu J, Liu JJ, et al. In vivo anticancer efficacy assessment with an imaging-based platform: taking Brucea javanica oil emulsion as an example. J Unexplored Med Data. 2016; 1: 21-29.
9. Ni Y, Marchal G, Zhang X, Van Hecke P, Michiels J, Yu J, et al. The uptake of manganese dipyridoxal-diphosphate by chemically induced hepatocellular carcinoma in rats. A correlation between contrast-media-enhanced magnetic resonance imaging, tumor differentiation, and vascularization. Invest Radiol. 1993; 28: 520-528.
10. Guzman G, Cotler SJ, Lin AY, Maniotis AJ, Folberg R. A Pilot Study of Vasculogenic Mimicry Immunohistochemical Expression in Hepatocellular Carcinoma. Arch Pathol Lab Med. 2007; 131: 1776-1781.
11. Ni Y, Marchal G, Van Damme B, Van Hecke P, Michiels J, Zhang X, et al. Magnetic Resonance Imaging, Microangiography, and Histology in a Rat Model of Primary Liver-Cancer. Invest Radiol. 1992; 27: 689-697.
12. Hanahan D, Weinberg RA. Hallmarks of Cancer: The Next Generation. Cell. 2011; 144: 646-674.
13. Paget S. The distribution of secondary growths in cancer of the breast. 1889. Cancer Metastasis Rev. 1989; 8: 98-101.
14. Fidler IJ. Metastasis: quantitative analysis of distribution and fate of tumor emboli labeled with 125 I-5-iodo-2'-deoxyuridine. J Natl Cancer Inst. 1970; 45: 773-782.
15. Fang ZT, Wang GZ, Zhang W, Qu XD, Liu R, Qian S, et al. Transcatheter arterial embolization promotes liver tumor metastasis by increasing the population of circulating tumor cells. Onco Targets Ther. 2013; 6: 1563-1572.
16. Hart IR, Easty D. Tumor cell progression and differentiation in metastasis. Semin Cancer Biol. 1991; 2: 87-95.
17. Clarke MF, Dick JE, Dirks PB, Eaves CJ, Jamieson CHM, Jones DL, et al. Cancer Stem Cells--Perspectives on Current Status and Future Directions: AACR Workshop on Cancer Stem Cells. Cancer Res. 2006; 66: 9339-9344.
18. Oishi N, Yamashita T, Kaneko S. Molecular biology of liver cancer stem cells. Liver Cancer. 2014; 3: 71-84.
19. Lingala S, Cui YY, Chen X, Ruebner BH, Qian XF, Zern MA, et al. Immunohistochemical staining of cancer stem cell markers in hepatocellular carcinoma. Exp Mol Pathol. 2010; 89: 27-35.
20. Lee JS, Chu IS, Mikaelyan A, Calvisi DF, Heo J, Reddy JK, et al. Application of comparative functional genomics to identify best-fit mouse models to study human cancer. Nat Genet. 2004; 36: 1306-1311.
21. Fidler IJ. The pathogenesis of cancer metastasis: the "seed and soil" hypothesis revisited. Nat Rev Cancer 2003; 3: 453-458.
22. Yamamoto J, Shimajiri S, Miyaoka R, Nishizawa S. Pitfalls of conservative treatments of multiple probable cerebral cavernous malformations (CCMs): clinicopathological features of CCMs coexisting with vasculogenic mimicry in an anaplastic oligodendroglioma. Brain Tumor Pathol. 2014; 31: 215-221.
23. Cao Z, Bao M, Miele L, Sarkar FH, Wang Z, Zhou Q. Tumour vasculogenic mimicry is associated with poor prognosis of human cancer patients: A systemic review and meta-analysis. Eur J Cancer. 2013; 49: 3914-3923.
24. Chen JA, Shi M, Li JQ, Qian CN. Angiogenesis: multiple masks in hepatocellular carcinoma and liver regeneration. Hepatol Int. 2010; 4: 537-547.
25. Liu Y, Yin T, Feng Y, Cona MM, Huang G, Liu J, et al. Mammalian models of chemically induced primary malignancies exploitable for imaging-based preclinical theragnostic research. Quant Imaging Med Surg. 2015; 5: 708-729.